Structural Engineering and Mechanics, *Vol. 63, No. 2 (2017) 225-235*
DOI: https://doi.org/10.12989/sem.2017.63.2.225

Dynamic behaviour of orthotropic elliptic paraboloid shells with openings

Kutlu Darılmaz*

Department of Civil Engineering, Istanbul Technical University, 34469 Maslak, Istanbul, Turkey

(Received August 11, 2016, Revised January 12, 2017, Accepted February 10, 2017)

Abstract. In this paper a vibration study on orthotropic elliptic paraboloid shells with openings is carried out by using a hybrid stress finite element. The formulation of the element is based on Hellinger-Reissner variational principle. The element is developed by combining a hybrid plane stress element and a hybrid plate element. Natural frequencies of orthotropic elliptic paraboloid shells with and without openings are presented. The influence of aspect ratio, height ratio, opening ratio and material angle on the frequencies and mode shapes are investigated.

Keywords: elliptic paraboloid shell;, shell; opening; assumed stress hybrid element; finite element; free vibration

1. Introduction

Elliptic paraboloid shells have been widely used in important aerospace, aircraft, industrial engineering and civil structural members which provide an optimal combination of minimum weight and necessary strength. Therefore, there are real, practical needs for investigating the behavior of these structures.

There have been extensive research carried out in the past years to investigate the behavior and design of circular shell structures but the literature on the analysis of non-circular shells is limited when compared with circular shells. Concerning the analysis of elliptic paraboloid type of non-circular shells, there is a much smaller amount of work. One of the earliest works in element formulations for the analysis of elliptical parabolic shells was reported by Aass (1963) who applied it to elliptic paraboloid shells. Mohraz and Schnobrich (1966) studied the analysis of shallow shell structures including elliptic paraboloid shells by a discrete element system. Chun *et al*. (2009) presented a shear deformable four-noded finite element based on a hybrid/mixed assumed stress for the analysis of anisotropic laminated elliptical and parabolic shells, and conducted a parametric study of anisotropic elliptical and parabolic shells of various configurations to investigate the effects of aspect and height ratios as well as layer lay-up schemes.

Shell and plate members often contain openings intended for certain reasons. These openings may significantly change the behavior of these members. A few references dealing with dynamic behavior of shells with openings or cutouts are available. Jullien and Limam (1998) studied the effects of openings on the stability problem of cylindrical shells with cutouts and also investigated the effect of the location and the number of the holes. Shariati and Rokhi (2010) carried out analysis of steel cylindrical shells with various diameter and length having an elliptical cutout subjected to axial compression and investigated the the influence of the cutout size, cutout angle and the shell aspect ratios on the pre-buckling, buckling, and post-buckling responses. Singh and Kumar (2010) investigated the effects of cutout shape (i.e., circular, square, diamond, elliptical-vertical and elliptical-horizontal) and size on buckling and post buckling response of quasi-isotropic composite laminate under uni-axial compression. Kang (2014) presented a three dimensional method of analysis for determining the free vibration frequencies of joined hemispherical-cylindrical shells of revolution with a top opening. Ghazijahani *et al*. (2014) investigated the effect of circular openings on the behavior and failure mode of circular hollow sections (CHS) members. Nicholas *et al*. (2014) studied the buckling optimization of laminated composite plates with elliptical cutout using artificial neural network, and explored the effectiveness of the proposed method. Torabi and Shariati (2014) studied the buckling of steel thin-walled semi-spherical shells with square cutout due to axial compressive loads, and determine the influence of the cut out size-to-location and the thickness-to-diameter on the mean collapse load of the semi-spherical shells. Chernobryvko *et al*. (2014) numerically analyzed the properties of eigen-frequencies and eigen-modes of parabolic shells by using the Rayleigh-Ritz method. Ghazijahani *et al*. (2015) investigated the structural behavior of tubes with door-shaped cutouts under axial loading and examined the buckling modes and effect of geometric parameters of a cutout. Kang (2015) presented a three-dimensional method of analysis for determining the free vibration frequencies of shallow or deep, clamped parabolic shells having variable thickness by the Ritz method. Xie *et al*. (2015) studied the free vibration analysis of functionally graded spherical and parabolic shells of revolution with arbitrary boundary conditions by using a Haar Wavelet Discretization method-based solution approach. Rajanna *et al*. (2016) investigated the influence of centrally placed circular and square cutouts on vibration and buckling characteristics of different ply-oriented

*Corresponding author, Professor
E-mail: darilmazk@itu.edu.tr

http://www.techno-press.com/journals/sem&subpage=7 ISSN: 1225-4568 (Print), 1598-6217 (Online)

laminated panels under the action of compressive and/or tensile types of non-uniform in-plane edge loads. Javed *et al*. (2016) studied the free vibration of antisymmetric angle-ply conical shells having non-uniform sinusoidal thickness variation for different support conditions. Darılmaz (2017) investigated the static and free vibration of orthotropic elliptic paraboloid shells.

The paper aims to investigate the free vibration response of orthotropic elliptic paraboloid shells with openings at the top with a parametric study by varying the aspect ratio, height ratio, opening ratio, and material angle.

It is well known that some of general shaped shells have been quite successfully solved by flat-shell elements of rectangular or quadrilateral shapes. For practical purposes, the behavior of a curved surface can be reasonably well approximated by using small flat elements. The flat element approximation also allows an easy coupling with the edge beams which sometimes difficult to implement in the curved element formulation. In this paper, a flat shell element which is a combination of membrane element and a plate element is used, based on the classical hybrid stress method which was first developed by Pian (1964). The element is generated by a combination of a hybrid plane stress element with drilling d.o.f. and a hybrid plate element. The validity and efficiency of the element can be found in previous studies of the author, Darılmaz (2007, 2012).

2. Element stiffness formulation

The assumed-stress hybrid method is based on the independent prescriptions of stresses within the element and displacements on the element boundary. The element stiffness matrix is obtained using Hellinger-Reissner variational principle. The Hellinger-Reissner functional of linear elasticity allows displacements and stresses to be varied separately. This establishes the master fields. Two slave strain fields appear, one coming from displacements and one from stresses.

The Hellinger-Reissner functional can be written as

$$\Pi_{RH} = \int_V \{\sigma\}^T [D]\{u\}\, dV - \frac{1}{2}\int_V \{\sigma\}^T [S]\{\sigma\}\, dV \tag{1}$$

where $\{\sigma\}$ is the stress vector, $[S]$ is the compliance matrix relating strains, $\{\varepsilon\}$, to stress ($\{\varepsilon\}=[S]\{\sigma\}$), $[D]$ is the differential operator matrix corresponding to the linear strain-displacement relations ($\{\varepsilon\}=[D]\{u\}$) and V is the volume of structure.

The approximation for stresses and displacements can now be incorporated in the functional. The stress field is described in the interior of the element as

$$\{\sigma\} = [P]\{\beta\} \tag{2}$$

and a compatible displacement field is described by

$$\{u\} = [N]\{q\} \tag{3}$$

where $[P]$ and $[N]$ are matrices of stress and displacement interpolation functions, respectively, and $\{\beta\}$ and $\{q\}$are the unknown stress and nodal displacement parameters, respectively. Intra-element equilibrating stresses and compatible displacements are independently interpolated. Since stresses are independent from element to element, the stress parameters are eliminated at the element level and a conventional stiffness matrix results. This leaves only the nodal displacement parameters to be assembled into the global system of equations.

Substituting the stress and displacement approximations Eq. (2), Eq. (3) in the functional Eq. (1) yields

$$\Pi_{RH} = [\beta]^T [G][q] - \frac{1}{2}[\beta]^T [H][\beta] \tag{4}$$

where

$$[H] = \int_V [P]^T [S][P]\, dV \tag{5}$$

$$[G] = \int [P]^T \left([D][N]\right) dV \tag{6}$$

Now imposing stationary conditions on the functional with respect to the stress parameters $\{\beta\}$ gives

$$[\beta] = [H]^{-1}[G]\ [q] \tag{7}$$

Substitution of $\{\beta\}$ in Eq. (4), the functional reduces to

$$\Pi_{RH} = \frac{1}{2}[q]^T [G]^T [H]^{-1}[G][q] = \frac{1}{2}[q]^T [K][q] \tag{8}$$

where

$$[K] = [G]^T [H]^{-1}[G] \tag{9}$$

is recognized as a stiffness matrix.

The solution of the system yields the unknown nodal displacements $\{q\}$. After $\{q\}$ is determined, element stresses or internal forces can be recovered by use of Eq. (7) and Eq. (2). Thus

$$\{\sigma\} = [P][H]^{-1}[G]\{q\} \tag{10}$$

3. Governing equations

Consider an elliptic paraboloid shell of uniform thickness which the orthotropic material property may be arbitrarily oriented at an angle ϕ with reference to the x-axis of the local coordinate system Fig. 1.

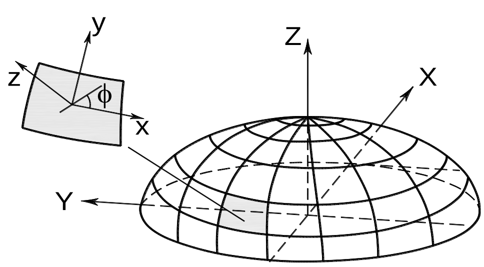

Fig. 1 Global and local axis of elliptic paraboloid shell

The stress-strain relation with respect to *x*, *y* and *z* axes can be written as

$$\begin{Bmatrix} \sigma_x \\ \sigma_y \\ \tau_{xy} \end{Bmatrix} = \begin{bmatrix} \bar{\Omega}_{11} & \bar{\Omega}_{12} & \bar{\Omega}_{16} \\ \bar{\Omega}_{12} & \bar{\Omega}_{22} & \bar{\Omega}_{26} \\ \bar{\Omega}_{16} & \bar{\Omega}_{26} & \bar{\Omega}_{66} \end{bmatrix} \begin{Bmatrix} \varepsilon_x \\ \varepsilon_x \\ \gamma_{xy} \end{Bmatrix} \quad \text{(i,j=1,2,6)} \tag{11}$$

$$\begin{Bmatrix} \tau_{xz} \\ \tau_{yz} \end{Bmatrix} = \begin{bmatrix} \bar{\Omega}_{44} & \bar{\Omega}_{45} \\ \bar{\Omega}_{45} & \bar{\Omega}_{55} \end{bmatrix} \begin{Bmatrix} \gamma_{xz} \\ \gamma_{yz} \end{Bmatrix} \tag{12}$$

.$\left[\bar{\Omega}_{ij}\right]$ in Eqs. (11) and (12) is defined as

$$\left[\bar{\Omega}_{ij}\right] = \left[T_1\right]^{-1}\left[\Omega_{ij}\right]\left[T_1\right]^{-T} \quad \text{(i,j=1,2,6)} \tag{13}$$

$$\left[\bar{\Omega}_{ij}\right] = \left[T_2\right]^{-1}\left[\Omega_{ij}\right]\left[T_2\right] \quad \text{(i,j=4,5)} \tag{14}$$

in which

$$\left[T_1\right] = \begin{bmatrix} \cos^2\phi & \sin^2\phi & 2\sin\phi\cos\phi \\ \sin^2\phi & \cos^2\phi & -2\sin\phi\cos\phi \\ -\sin\phi\cos\phi & \sin\phi\cos\phi & \cos^2\phi - \sin^2\phi \end{bmatrix} \tag{15}$$

$$\left[T_2\right] = \begin{bmatrix} \cos\phi & -\sin\phi \\ \sin\phi & \cos\phi \end{bmatrix} \tag{16}$$

$$\left[\Omega_{ij}\right] = \begin{bmatrix} \Omega_{11} & \Omega_{12} & 0 \\ \Omega_{12} & \Omega_{22} & 0 \\ 0 & 0 & \Omega_{66} \end{bmatrix} \quad \text{(i,j=1,2,6)} \tag{17a}$$

$$\left[\Omega_{ij}\right] = \begin{bmatrix} \Omega_{44} & 0 \\ 0 & \Omega_{55} \end{bmatrix} \quad \text{(i,j=4,5)} \tag{17b}$$

$$\Omega_{11} = \frac{E_1}{1-\nu_{12}\nu_{21}} \quad \Omega_{12} = \frac{\nu_{12}E_2}{1-\nu_{12}\nu_{21}} \qquad \Omega_{22} = \frac{E_2}{1-\nu_{12}\nu_{21}} \tag{18a}$$

$$\Omega_{66} = G_{12} \qquad \Omega_{44} = G_{13} \qquad \Omega_{55} = G_{23} \tag{18b}$$

$$G_{ij} = \frac{\sqrt{E_i E_j}}{2\left(1+\sqrt{\nu_{ij}\nu_{ji}}\right)} \quad \text{(i,j=1,2,3)} \tag{18c}$$

The stress resultants are given by

$$\begin{bmatrix} N_x & M_x \\ N_y & M_y \\ N_{xy} & M_{xy} \end{bmatrix} = \int_{-h/2}^{h/2} \begin{bmatrix} \sigma_x \\ \sigma_y \\ \tau_{xy} \end{bmatrix} \left[1 \quad z\right] dz \quad \text{(i,j=1,2,3)} \tag{19a}$$

$$\begin{bmatrix} Q_x \\ Q_y \end{bmatrix} = \int_{-h/2}^{h/2} \begin{bmatrix} \tau_{xz} \\ \tau_{yz} \end{bmatrix} dz \quad \text{(i,j=1,2,3)} \tag{19b}$$

From Eqs. (19a) and (19b) the constitutive equations of the elliptic paraboloid shell are obtained as

$$\{F\} = [E]\{\chi\} \quad \text{(i,j=1,2,3)} \tag{20}$$

where

$$\{F\} = \left\{N_x, N_y, N_{xy}, M_x, M_y, M_{xy}, Q_x, Q_y\right\} \tag{21}$$

$$\{\chi\} = \left\{\varepsilon_x, \varepsilon_y, \gamma_{xy}, \kappa_x, \kappa_y, \kappa_{xy}, \gamma_{xz}, \gamma_{yz}\right\} \tag{22}$$

The elasticity matrix can be expressed as

$$[E] = \begin{bmatrix} \left[A_{ij}\right] & \left[B_{ij}\right] & 0 \\ \left[B_{ij}\right] & \left[C_{ij}\right] & 0 \\ 0 & 0 & \left[D_{ij}\right] \end{bmatrix} \tag{23}$$

in which

$$\left[A_{ij}\right] = \int_{-h/2}^{h/2} \left[\bar{\Omega}_{ij}\right] dz, \quad \left[B_{ij}\right] = \int_{-h/2}^{h/2} \left[\bar{\Omega}_{ij}\right] z\, dz, \qquad \left[C_{ij}\right] = \int_{-h/2}^{h/2} \left[\bar{\Omega}_{ij}\right] z^2 dz \quad \text{(i,j=1,2,6)} \tag{24.a}$$

$$\left[D_{ij}\right] = \int_{-h/2}^{h/2} \left[\bar{\Omega}_{ij}\right] dz \quad \text{(i,j=4,5)} \tag{24.b}$$

4. The hybrid stress element

The element is generated by a combination of a hybrid membrane element and a hybrid plate element.

4.1 Membrane component of the element with drilling degree of freedom

Generally membrane elements have two translational d.o.f (u,v) per node but the need for membrane elements with a drilling degree of freedom arises in many engineering problems. A drilling rotation is defined as inplane rotation about the axis normal to the plane of element. This type of element is useful in solving folded plate structures and provides an easy coupling with edge beams which have six d.o.f per node. Inclusion of a drilling degree of freedom gives also the improved behavior of the element (Allman 1984). The possibility of membrane elements with drilling d.o.f was opened by Allman (1984), Bergan and Felippa (1985). The concept has been further elaborated by many other researchers (Cook 1986, MacNeal and Harder 1988, Yunus *et al*. 1989, Ibrahimbegovic *et al*. 1990, Choi and Lee 1996) for more improved elements.

Formulation of drilling d.o.f for the present element is based on the procedure given by Yunus *et al*. (1989). The displacement fields are expressed in terms of translational and rotational d.o.f.'s at the corner nodes only.

The membrane displacement field for the 4-node element is derived from an 8-node element, Fig. 2.

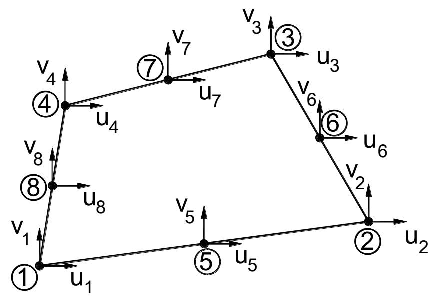

(a) 8-node membrane

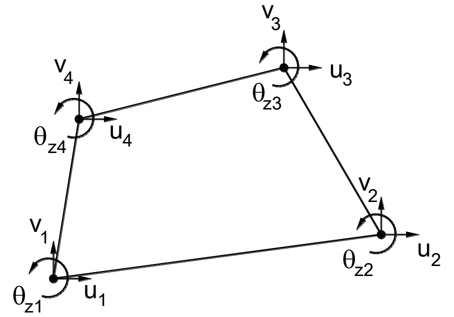

(b) 4-node membrane

Fig. 2 Displacements

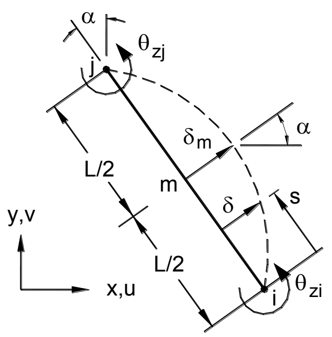

Fig. 3 Side displacement produced by drilling degrees of freedoms θ_{zi} and θ_{zj}

Rotational d.o.f. are associated with parabolic displaced shapes of element sides. In Fig. 3, rotational d.o.f. θ_{zi} and θ_{zj} are shown at nodes *i* and *j* of the element side of length *L*.

δ can be regarded as quadratic in side-tangent coordinates. θ_{zi} and θ_{zj} produce the edge normal displacement δ and midside value δ_m

$$\delta = \frac{s(L-s)}{2L}\left(\theta_{zi}-\theta_{zj}\right) \qquad \delta_m = \frac{L}{8}\left(\theta_{zi}-\theta_{zj}\right) \tag{25}$$

The *x* and *y* components of δ are $\delta\cos\alpha$ and $\delta\sin\alpha$. Therefore, after adding the contribution to displacement from nodes *i* and *j*, the total displacements *u* and *v* of a typical point on the edge are

$$\begin{Bmatrix} u \\ v \end{Bmatrix} = \frac{L-s}{L}\begin{Bmatrix} u_i \\ v_i \end{Bmatrix} + \frac{s}{L}\begin{Bmatrix} u_j \\ v_j \end{Bmatrix} + \frac{(L-s)s}{2L}\left(\theta_{zj}-\theta_{zi}\right)\begin{Bmatrix} \cos\alpha \\ \sin\alpha \end{Bmatrix} \tag{26}$$

Side 1-5-2 of the element, Fig. 2 d.o.f. at node 5 are related to d.o.f. at nodes 1 and 2 of the element. By evaluating Eq. (26) with $s=L/2$ with $i=1$, $j=2$, $L\cos\alpha=y_2-y_1$ and $L\sin\alpha=x_2-x_1$, yields

$$\begin{Bmatrix} u_5 \\ v_5 \end{Bmatrix} = \frac{1}{2}\begin{Bmatrix} u_1 \\ v_1 \end{Bmatrix} + \frac{1}{2}\begin{Bmatrix} u_2 \\ v_2 \end{Bmatrix} + \frac{\left(\theta_{zj}-\theta_{zi}\right)}{8}\begin{Bmatrix} y_2-y_1 \\ x_1-x_2 \end{Bmatrix} \tag{27}$$

After doing the same for d.o.f. at nodes 6, 7 and 8 d.o.f. in Fig. 2(a) and (b) by the transformation, the complete relation can be written

$$\left\{u_1 \quad v_1 \quad ..... \quad u_8 \quad v_8\right\}^T = \left[T\right]_{16x12}\left\{q\right\}^T_{membrane} \tag{28}$$

where

$$\left\{q\right\}_{membrane} = \left\{u_1 \quad v_1 \quad \theta_{z1} \quad ... \quad u_4 \quad v_4 \quad \theta_{z4}\right\}_{1x12} \tag{29}$$

So the midside nodal displacements can be written in terms of the corner nodal displacements and rotations and the displacement field for the 4-node, twelve d.o.f. membrane element can be derived from an 8-node membrane element. This is done through the use of the transformation matrix [*T*]. The form of [*T*] is given in Appendix.

The biggest difficulty in deriving hybrid finite elements seems to be the lack of a rational methodology for deriving stress terms, Feng *et al*. (1997). It is recognized that the number of stress modes m in the assumed stress field should satisfy

$$m \geq n-r \tag{30}$$

with *n* the total number of nodal displacements, and *r* the number of rigid body modes in an element. If Eq. (30) is not satisfied, use of too few coefficients in $\{\beta\}$, the rank of the element stiffness matrix will be less than the total degrees of deformation freedom and the numerical solution of the finite element model will not be stable and produces on element with one or more mechanism.

Increasing the number of β's by adding stress modes of higher-order term, each extra term will add more stiffness and stiffens the element, Pian and Chen (1983), Punch and Atluri (1984), Darılmaz (2006).

The assumed stress field for the membrane part which satisfies the equilibrium conditions for zero body forces and avoid rank deficiency is given as

$$\begin{aligned} N_x &= \beta_1+\beta_2 x+\beta_3 y+\beta_4 x^2+\beta_5 xy+\beta_6 y^2 \\ N_y &= \beta_4 y^2+\beta_7+\beta_8 x+\beta_9 y+\beta_{10} x^2+\beta_{11} xy \\ N_{xy} &= -\beta_2 y-2\beta_4 xy-\beta_5 y^2/2-\beta_9 x-\beta_{11} x^2/2+\beta_{12} \end{aligned} \tag{31}$$

4.1 Plate component of the element

The flexural component of the element is identical to that of the plate bending element presented by the author, Darılmaz (2005), and corresponds to the Mindlin/Reissner plate theory. Only the assumed stress field which satisfies the equilibrium conditions for the plate part is given here

$$M_x = \beta_1+\beta_4 y+\beta_6 x+\beta_8 xy \tag{32}$$

$$M_y = \beta_2 + \beta_5 x + \beta_7 y + \beta_9 xy$$
$$M_{xy} = \beta_3 + \beta_{10} x + \beta_{11} y + \beta_{12} x^2/2 + \beta_{13} y^2/2$$
$$Q_x = \beta_6 + \beta_{11} + \beta_8 y + \beta_{13} y$$
$$Q_y = \beta_7 + \beta_{10} + \beta_9 x + \beta_{12} x$$

The nodal displacements for the plate are chosen as

$$\{q\}_{plate} = \{w_1 \quad \theta_{x1} \quad \theta_{y1} \quad \dots \quad w_4 \quad \theta_{x4} \quad \theta_{y4}\}_{1x12} \tag{33}$$

The combination of membrane and plate element yields the element which has 6 d.o.f per node and totally 24 d.o.f .

3. Element mass matrix

The problem of determination of the natural frequencies of vibration of a plate reduces to the solution of the standard eigenvalue problem $[K]-\omega^2[M]=0$, where ω is the natural circular frequency of the system. Making use of the conventional assemblage technique of the finite element method with the necessary boundary conditions, the system matrix $[K]$ and the mass matrix $[M]$ for the entire structure can be obtained.

Element consistent mass matrix is derived from the kinetic energy expression, Cook *et al*. (2001)

$$E_k = \frac{1}{2}\int \rho \{\dot{q}\}^T \{\dot{q}\} dV \tag{34}$$

where $\{\dot{q}\}$ denotes the velocity components.

The nodal and generalized velocity vectors are related with the help of shape functions

$$\{\dot{q}\} = \sum_{i=1}^{4} [N]\{\dot{q}_i\} \tag{35}$$

Substituting the velocity vectors in the kinetic energy, Eq. (34) yields the mass matrix of an element.

$$E_k = \frac{1}{2}\int_V \rho \{\dot{q}_i\}^T [N]^T [N]\{\dot{q}_i\} dV \tag{36}$$

$$E_k = \frac{1}{2}\int_A \{\dot{q}_i\}^T [m]\{\dot{q}_i\} dA \tag{37}$$

where $[m]$ is the element consistent mass matrix and is given by

$$[m] = \int_V \rho [N]^T [N] dV \tag{38}$$

3. Numerical study

An orthotropic elliptical paraboloid shell with major axis a and minor axis b and height h shown in Fig. 4 is considered. The shell has an elliptical opening at the top center with major axis a1 and minor axis b1. Material properties are chosen as, E_1=60.7×10^9 N/m^2, E_2=24.8×10^9 N/m^2, $G_{12}=G_{13}=G_{23}=12\cdot 10^9$ N/m^2, $\nu_{12}=\nu_{21}=0.23$, ρ=1300 kg/m^3 where E_1 and E_2 are the modulus of elasticity along x and y axes of element, G_{ij} is the shear modulus and ν_{ij} is Poisson's ratio, respectively.

A parametric study is carried out to investigate the influence of aspect ratio (a/b), height ratio (h/b), opening ratio (a_1/a), and material angle (ϕ) on free vibration behavior of orthotropic elliptic paraboloid shells with opening at the top. For a reference solution an elliptic paraboloid shell without opening is also considered.

The aspect ratio, a/b, of elliptical shell is taken as the ratio of the radius length of X-axis to that of Y-axis. Whereas, the height ratio h/b, of elliptical shell is taken as the radius length of Z-axis divide into that of Y-axis.

The elliptical paraboloid shells are analyzed by varying the aspect ratio (a/b=0.25, 0.50 and 1.0), height ratio (h/b=0.25, 0.50 and 1.0), opening ratio (a_1/a=0, 0.25, 0.50 and 0.75) and material angle (ϕ=0°, 45°, 90°). The relative total mass ratios of elliptic paraboloid shells are given in Table 1, and the shell for a/b=1, h/b=1 and a_1/a=0 is taken as the reference shell.

The natural frequencies are normalized by

$$\varpi = \omega b\sqrt{\rho\left(1-\nu_{21}^2\right)/E_1} \tag{39}$$

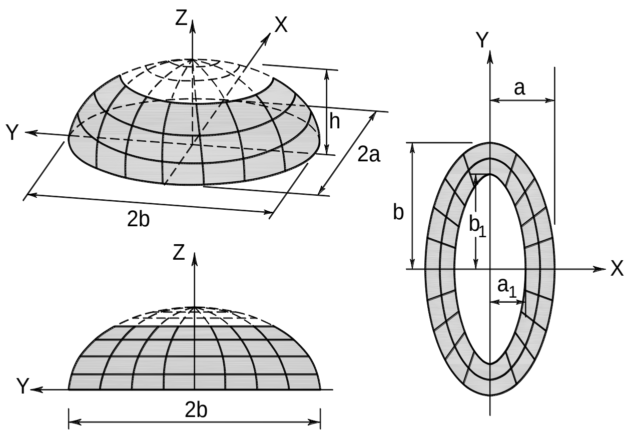

Fig. 4 Geometry of elliptic paraboloid shell

Table 1 Relative total mass ratios for elliptic paraboloid shells

		a/b=1			*a/b*=0.5			*a/b*=0.25		
	h/b	0.25	0.5	1.0	0.25	0.5	1.0	0.25	0.5	1.0
a_1/a										
0		0.62	0.72	1.00	0.34	0.43	0.69	0.21	0.32	0.56
0.25		0.59	0.68	0.96	0.32	0.41	0.67	0.20	0.30	0.55
0.50		0.48	0.56	0.82	0.26	0.35	0.58	0.16	0.26	0.49
0.75		0.28	0.34	0.52	0.16	0.22	0.37	0.10	0.17	0.32

Table 2 Non-dimensional natural frequencies ϖ for elliptic paraboloid shell (a_1/a=0)

		a/b=1			*a/b*=0.5			*a/b*=0.25		
	h/b	0.25	0.5	1.0	0.25	0.5	1.0	0.25	0.5	1.0
ϕ	Mode									
0°	1	0.334	0.436	0.346	0.429	0.486	0.300	0.430	0.325	0.194
	2	0.334	0.436	0.346	0.461	0.491	0.301	0.462	0.332	0.199
	3	0.339	0.443	0.348	0.487	0.511	0.301	0.613	0.389	0.206
	4	0.339	0.443	0.348	0.512	0.515	0.303	0.651	0.409	0.214
	5	0.342	0.444	0.364	0.530	0.520	0.355	0.667	0.414	0.251
45°	1	0.318	0.451	0.361	0.379	0.415	0.300	0.378	0.294	0.185
	2	0.318	0.451	0.361	0.397	0.431	0.302	0.469	0.297	0.189
	3	0.323	0.451	0.362	0.462	0.479	0.306	0.629	0.393	0.210
	4	0.323	0.451	0.362	0.511	0.502	0.307	0.636	0.395	0.215
	5	0.335	0.458	0.375	0.549	0.511	0.336	0.729	0.421	0.237
90°	1	0.334	0.479	0.393	0.363	0.407	0.309	0.387	0.297	0.186
	2	0.334	0.479	0.393	0.404	0.429	0.310	0.515	0.297	0.187
	3	0.334	0.513	0.394	0.486	0.471	0.316	0.638	0.404	0.210
	4	0.339	0.513	0.394	0.526	0.529	0.317	0.668	0.415	0.214
	5	0.339	0.515	0.400	0.545	0.530	0.337	0.831	0.438	0.235

Table 3 Non-dimensional natural frequencies ϖ for elliptic paraboloid shell (a_1/a=0.25)

		a/b=1			*a/b*=0.5			*a/b*=0.25		
	h/b	0.25	0.5	1.0	0.25	0.5	1.0	0.25	0.5	1.0
ϕ	Mode									
0°	1	0.203	0.255	0.222	0.314	0.309	0.212	0.339	0.239	0.156
	2	0.203	0.255	0.222	0.347	0.349	0.233	0.433	0.316	0.183
	3	0.283	0.339	0.308	0.460	0.458	0.296	0.435	0.326	0.193
	4	0.283	0.339	0.308	0.474	0.483	0.298	0.578	0.377	0.205
	5	0.335	0.436	0.346	0.479	0.501	0.305	0.586	0.407	0.227
45°	1	0.182	0.236	0.215	0.270	0.271	0.196	0.313	0.208	0.138
	2	0.182	0.236	0.215	0.322	0.328	0.224	0.375	0.289	0.171
	3	0.251	0.292	0.269	0.383	0.396	0.286	0.412	0.299	0.183
	4	0.251	0.292	0.269	0.428	0.430	0.294	0.547	0.364	0.205
	5	0.319	0.423	0.361	0.436	0.474	0.311	0.569	0.392	0.224
90°	1	0.172	0.232	0.225	0.258	0.261	0.200	0.318	0.202	0.132
	2	0.172	0.232	0.225	0.309	0.328	0.238	0.373	0.289	0.177
	3	0.233	0.267	0.246	0.365	0.379	0.290	0.417	0.302	0.182
	4	0.233	0.267	0.246	0.411	0.407	0.302	0.553	0.357	0.204
	5	0.318	0.435	0.392	0.418	0.457	0.314	0.591	0.397	0.216

The five lowest normalized natural frequencies are evaluated by varying the parameters stated earlier, and the results are given in Table 2 to Table 5.

It can be observed that an increase in opening ratio lowers the fundamental frequency of the shell over $a_1/a \le 0.5$ and then raised. It may be deduced that for the opening ratios $a_1/a \le 0.5$, the change of stiffness is more effective than change of mass on frequencies. As the opening ratio is increasing the variation in frequency is decreasing and it may be said that the removed inertia and removed stiffness due to the presence of opening are almost self-cancelling in the vicinity of $0.5 < a_1/a < 0.75$.

Furthermore, it is evident from Fig. 5-Fig. 13 that the opening ratios considered are significantly affect the mode shapes. For all type of shells, lowest frequencies obtained for the case *h/b*=1, *a/b*=0.25.

The variation of frequency with material angle is less sensitive than the other parameters. Generally it has a tendency to decrease in shells with openings ($a_1/a > 0$). For shells without openings or having small opening ratios ($a_1/a \le 0.25$) and aspect ratios for $a/b \ge 0.5$, higher (i.e., fifth) mode frequencies increase with material angle.

For shells with openings, frequencies increase over aspect ratio $0.25 < a/b < 0.5$, and then decrease. The lowest

Table 4 Non-dimensional natural frequencies ϖ for elliptic paraboloid shell (a_1/a=0.25)

		a/b=1			*a/b*=0.5			*a/b*=0.25		
	h/b	0.25	0.5	1.0	0.25	0.5	1.0	0.25	0.5	1.0
ϕ	Mode									
0°	1	0.176	0.206	0.175	0.271	0.251	0.17	0.262	0.202	0.128
	2	0.176	0.206	0.175	0.275	0.254	0.171	0.27	0.208	0.14
	3	0.198	0.214	0.176	0.308	0.283	0.209	0.306	0.213	0.146
	4	0.198	0.214	0.176	0.326	0.288	0.217	0.365	0.267	0.168
	5	0.262	0.281	0.25	0.366	0.376	0.271	0.443	0.327	0.226
45°	1	0.165	0.184	0.156	0.246	0.232	0.159	0.22	0.181	0.121
	2	0.165	0.184	0.156	0.254	0.238	0.16	0.226	0.182	0.123
	3	0.175	0.204	0.172	0.262	0.249	0.185	0.285	0.195	0.127
	4	0.175	0.204	0.172	0.289	0.256	0.189	0.322	0.238	0.157
	5	0.232	0.239	0.212	0.322	0.327	0.248	0.401	0.283	0.203
90°	1	0.153	0.169	0.145	0.233	0.225	0.159	0.205	0.171	0.114
	2	0.153	0.169	0.145	0.246	0.231	0.161	0.209	0.173	0.119
	3	0.153	0.201	0.18	0.247	0.232	0.17	0.278	0.19	0.12
	4	0.153	0.201	0.18	0.272	0.236	0.172	0.304	0.224	0.15
	5	0.204	0.213	0.186	0.305	0.315	0.252	0.392	0.269	0.185

Table 5 Non-dimensional natural frequencies ϖ for elliptic paraboloid shell (a_1/a=0.75)

		a/b=1			*a/b*=0.5			*a/b*=0.25		
	h/b	0.25	0.5	1.0	0.25	0.5	1.0	0.25	0.5	1.0
ϕ	Mode									
0°	1	0.239	0.265	0.216	0.329	0.298	0.209	0.263	0.224	0.155
	2	0.239	0.265	0.216	0.33	0.3	0.21	0.263	0.226	0.155
	3	0.256	0.27	0.222	0.34	0.302	0.211	0.32	0.24	0.158
	4	0.256	0.27	0.222	0.34	0.304	0.212	0.32	0.243	0.159
	5	0.257	0.298	0.26	0.409	0.398	0.308	0.405	0.318	0.233
45°	1	0.229	0.254	0.206	0.272	0.273	0.195	0.209	0.188	0.139
	2	0.229	0.254	0.206	0.272	0.274	0.195	0.209	0.189	0.141
	3	0.239	0.264	0.212	0.298	0.277	0.196	0.279	0.215	0.145
	4	0.239	0.264	0.212	0.298	0.278	0.197	0.279	0.216	0.148
	5	0.24	0.271	0.228	0.348	0.345	0.268	0.359	0.273	0.202
90°	1	0.206	0.228	0.19	0.247	0.252	0.181	0.191	0.172	0.129
	2	0.206	0.228	0.19	0.248	0.252	0.182	0.191	0.172	0.131
	3	0.212	0.236	0.2	0.275	0.256	0.183	0.258	0.2	0.135
	4	0.212	0.236	0.2	0.275	0.257	0.184	0.258	0.2	0.138
	5	0.219	0.245	0.209	0.322	0.318	0.249	0.335	0.253	0.186

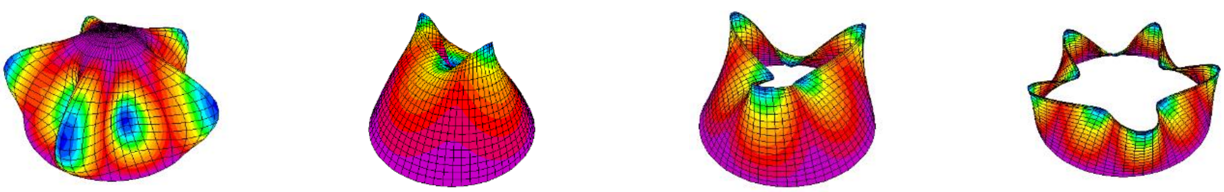

a_1/a=0 a_1/a=0.25 a_1/a=0.50 a_1/a=0.75

Fig. 5 First mode shapes of elliptic paraboloid shell (*a/b*=1, *h/b*=1, ϕ=0)

fundamental frequencies obtained for opening ratio a_1/a=0.5 for all aspect ratios.

For *a/b*=1, frequencies increase over 0.25≤*h/b*<0.5, and then decrease. Similar behavior can be observed for aspect ratio *a/b*=0.5 for the elliptic paraboloid shells without opening.

The mode shapes of the elliptic paraboloid shells considered are given in Fig. 5 to Fig. 13. For the sake of

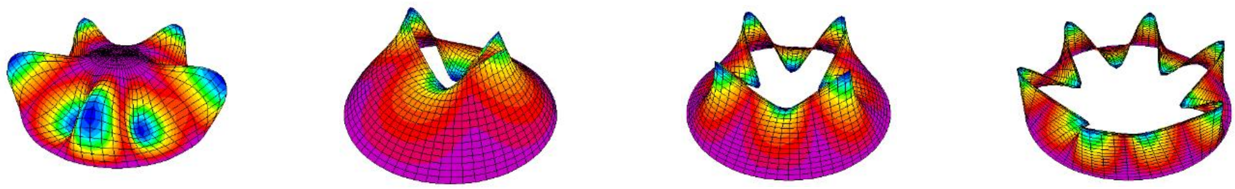

a_1/a=0 a_1/a=0.25 a_1/a=0.50 a_1/a=0.75

Fig. 6 First mode shapes of elliptic paraboloid shell (a/b=1, h/b=0.5, ϕ=0)

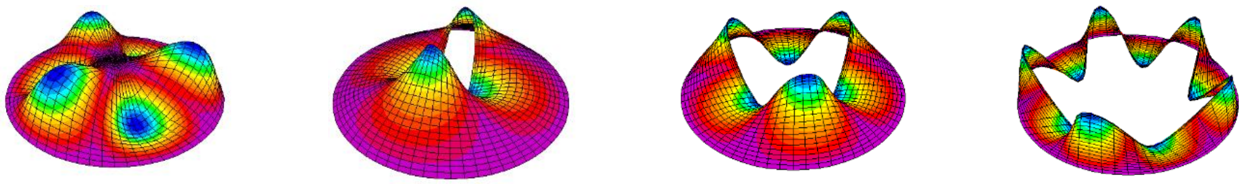

a_1/a=0 a_1/a=0.25 a_1/a=0.50 a_1/a=0.75

Fig. 7 First mode shapes of elliptic paraboloid shell (a/b=1, h/b=0.25, ϕ=0)

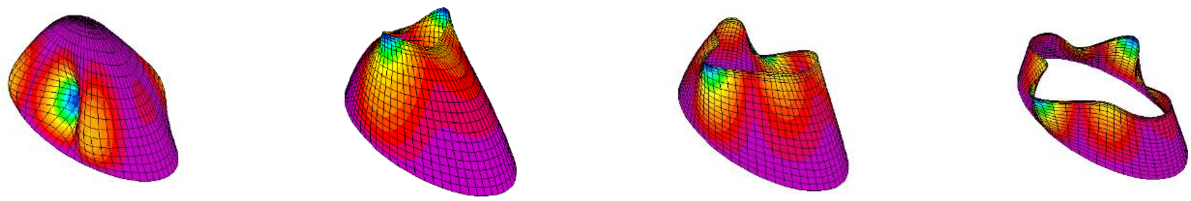

a_1/a=0 a_1/a=0.25 a_1/a=0.50 a_1/a=0.75

Fig. 8 First mode shapes of elliptic paraboloid shell (a/b=0.5, h/b=1, ϕ=0)

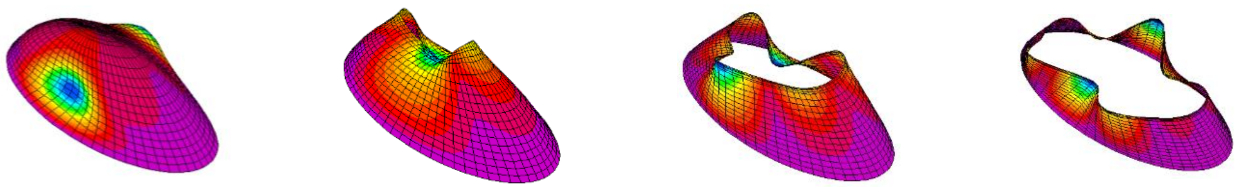

a_1/a=0 a_1/a=0.25 a_1/a=0.50 a_1/a=0.75

Fig. 9 First mode shapes of elliptic paraboloid shell (a/b=0.5, h/b=0.5, ϕ=0)

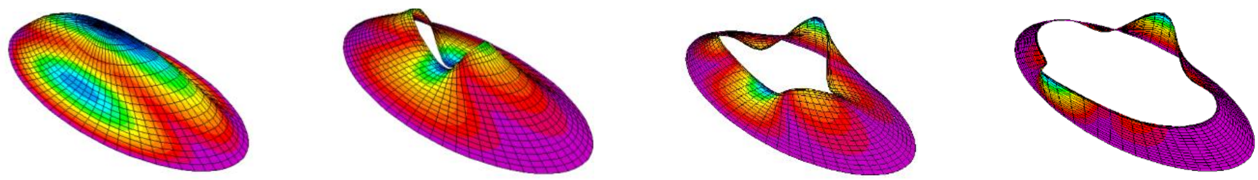

a_1/a=0 a_1/a=0.25 a_1/a=0.50 a_1/a=0.75

Fig. 10 First mode shapes of elliptic paraboloid shell (a/b=0.5, h/b=0.25, ϕ=0)

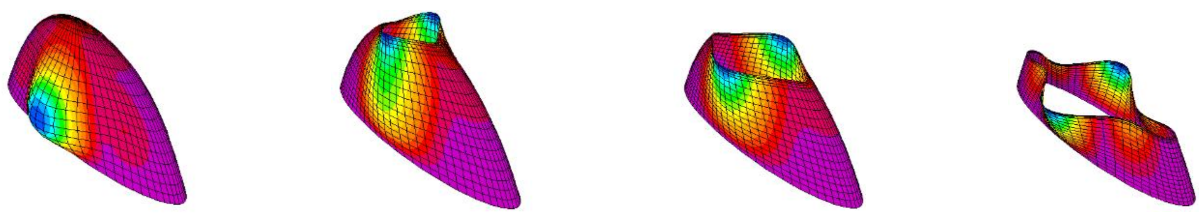

a_1/a=0 a_1/a=0.25 a_1/a=0.50 a_1/a=0.75

Fig. 11 First mode shapes of elliptic paraboloid shell (a/b=0.25, h/b=1, ϕ=0)

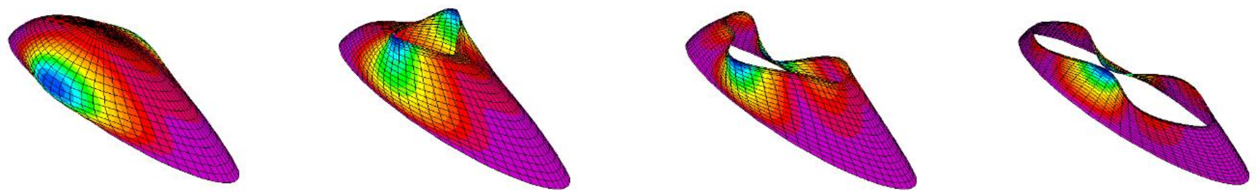

a_1/a=0 a_1/a=0.25 a_1/a=0.50 a_1/a=0.75

Fig. 12 First mode shapes of elliptic paraboloid shell (a/b=0.25, h/b=0.5, ϕ=0)

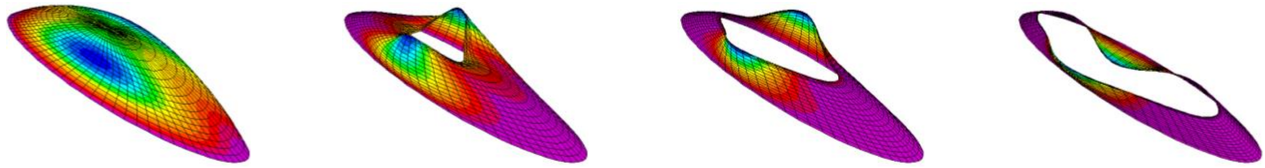

a_1/a=0 a_1/a=0.25 a_1/a=0.50 a_1/a=0.75

Fig. 13 First mode shapes of elliptic paraboloid shell (a/b=0.25, h/b=0.25, ϕ=0)

brevity mode shapes are shown in Figs. 5-13 for the first modes and material angle $\phi=0^{o}$ only.

5. Conclusions

An assumed stress hybrid finite element is used for the free vibration analysis of elliptic paraboloid shells with and without openings. A parametric study is carried out to investigate the influence of aspect ratio, height ratio, opening ratio and material angle on the dynamic behavior of elliptic paraboloid shells. Based on the above parametric study, the following concluding remarks are made:

Natural frequencies are more sensitive to aspect ratio, height ratio and opening ratio than material angle.

For all type of shells, with or without openings, lowest frequencies obtained for the case h/b=1, a/b=0.25.

As the opening ratio is increasing the variation in frequency is decreasing.

Opening ratios considered are significantly affect the mode shapes.

It is concluded that aspect ratio, height ratio and opening ratio of the cutout affect the free vibration behavior orthotropic elliptic paraboloid shells. For the design of elliptic paraboloid shells, the variation of frequencies with the aspect ratio a/b, height ratio h/b and opening ratio is presented in tables that can be directly used in design practice.

References

Aass, A. (1963), "A contribution to the bending theory of elliptic paraboloid shells", IABSE, 23.

Allman, D.J. (1984), "A compatible triangular element including vertex rotations for plane elasticity problems", *Comput. Struct.*, **19**, 1-8.

Bergan, P.G. and Felippa, C.A. (1985), "A triangular membrane element with rotational degrees of freedom", *Comput. Meth. Appl. Mech. Eng.*, **50**, 25-69.

Choi, C.K. and Lee, W.H. (1996), "Versatile variable-node flat-shell element", *J. Eng. Mech.*, **122**(5), 432-441.

Chun, K.S., Kassegne, S.K. and Wondimu, B.K. (2009), "Hybrid/mixed assumed stress element for anisotropic laminated elliptical and parabolic shells", *Finite Elem. Anal. Des.*, **45**(11), 766-781.

Cook, R.D. (1986), "On the Allman triangle and a related quadrilateral element", *Comput. Struct.*, **22**, 1065-1067.

Cook, R.D., Malkus D.S. and Plesha, M.E. (2001), *Concepts and Applications of Finite Element Analysis*, 4th Edition, Wiley.

Chernobryvko, M.V., Avramov, K.V., Romanenko, V.N., Batutina, T.J. and Tonkonogenko, A.M. (2014), "Free linear vibrations of thin axisymmetric parabolic shells", *Meccanica*, **49**(12), 2839-2845.

Darılmaz, K. (2005), "An assumed-stress finite element for static and free vibration analysis of Reissner-Mindlin plates", *Struct. Eng. Mech.*, **19**(2), 199-215.

Darılmaz, K. and Kumbasar, N. (2006), "An 8-node assumed stress hybrid element for analysis of shells", *Comput. Struct.*, **84**, 1990-2000.

Darılmaz, K. (2007), "An assumed-stress hybrid element for static and free vibration analysis of folded plates", *Struct. Eng. Mech.*, **25**(4), 405-421.

Darılmaz, K. (2012), "Stiffened orthotropic corner supported hypar shells: Effect of stiffener location, rise/span ratio and fiber orientaton on vibration behavior", *Steel Compos. Struct.*, **12**(4), 275-289.

Darılmaz, K. (2017), "Static and free vibration behaviour of orthotropic elliptic paraboloid shells", *Steel Compos. Struct.*, **23**(6), 737-746.

Feng, W., Hoa, S.V. and Huang, Q. (1997), "Classification of stress modes in assumed stress fields of hybrid finite elements", *Int. J. Num. Meth. Eng.*, **40**(23), 4313-4339.

Ghazijahani, T.G., Jiao, H. and Holloway, D. (2014), "Influence of a cutout on circular steel hollow sections under cyclic loading", *J. Constr. Steel Res.*, **100**, 12-20.

Ghazijahani, T.G., Jiao, H. and Holloway, D. (2015), "Structural behavior of shells with different cutouts under compression: An experimental study", *J. Constr. Steel Res.*, **105**, 129-137.

Ibrahimbegovic, A., Taylor, R.L. and Wilson, E.L. (1990), "A robust quadrilateral membrane finite element with drilling degrees of freedom", *Int. J. Numer. Meth. Eng.*, **30**(3), 445-457.

Javed, S., Viswanathan, K.K., Aziz, Z.A. and Lee, J.H. (2016), "Vibration analysis of a shear deformed anti-symmetric angle-ply conical shells with varying sinusoidal thickness", *Struct. Eng. Mech.*, 58(6), 1001-1020.

Jullien, J.F. and Limam, A. (1998), "Effects of openings of the buckling of cylindrical shells subjected to axial compression",

Thin Wall. Struct., **31**, 187-202
Kang, J.H. (2014), "Free vibrations of combined hemispherical-cylindrical shells of revolution with a top opening", *Int. J. Struct. Stab. Dyn.*, **14**(1), 1350023.
Kang, J.H. (2015), "Vibration analysis of shallow or deep, complete parabolic shells with variable thickness", *KSCE J. Civil Eng.*, **19**(7), 2172-2178.
MacNeal, R.H. and Harder, R.L. (1988), "A refined four-noded membrane element with rotational degrees of freedom", *Comput. Struct*., **28**, 75-84.
Mohraz, B. and Schnobrich, W.C. (1966), "The analysis of shallow shell structures by a discrete element system", Civil Engineering Studies, Structural Research Series No: 304.
Nicholas, P.E., Padmanaban, K.P. and Vasudevan, D. (2014), "Buckling optimization of laminated composite plate with elliptical cutout using ANN and GA", *Struct. Eng. Mech*., **52**(4), 815-827.
Pian, T.H.H. (1964), "Derivation of element stiffness matrices by assumed stress distributions", *AIAA J*., **12**, 1333-1336.
Pian, T.H.H. and Chen, D.P. (1983), "On the suppression of zero energy deformation modes", *Int. J. Numer. Meth. Eng*., **19**, 1741-1752.
Punch, E.F. and Atluri, S.N. (1984), "Development and testing of stable, isoparametric curvilinear 2 and 3-D hybrid stress elements", *Comput. Meth. Appl. Mech. Eng*., **47**, 331-356.
Shariati, M. and Rokhi, MM, (2010), "Buckling of steel cylindrical shells with an elliptical cutout", *Int. J. Steel Struct*., **10**(2), 193-205.
Rajanna, T., Banerjee, S., Desai, Y.M. and Prabhakara, D.L. (2016), "Vibration and buckling analyses of laminated panels with and without cutouts under compressive and tensile edge loads", *Steel Compos. Struct*., **21**(1), 37-55.
Singh, S.B. and Kumar, D. (2010), "Cutout shape and size effects on response of quasi-isotropic composite laminate under uni-axial compression", *Struct. Eng. Mech*., **35**(3), 335-348.
Torabi, H. and Shariati, M. (2014), "Buckling analysis of steel semi-spherical shells with square cutout under axial compression", *Streng. Mater*., **46**(4), 531-542.
Xie, X., Zheng, H. and Jin, G. (2015), "Free vibration of four-parameter functionally graded spherical and parabolic shells of revolution with arbitrary boundary conditions", *Compos. Part B: Eng.*, **77**, 59-73.
Yunus, S.M., Saigal, S. and Cook, R.D. (1989), "On improved hybrid finite elements with rotational degrees of freedom", *Int. J. Numer. Meth. Eng*., **28**(4), 785-800.

CC

Notations

E_1, E_2	: moduli of elasticity along *x* and *y* axes of element respectively
G_{12}, G_{13}, G_{23}	: shear moduli of elasticity in *x*-*y*, *x*-*z* and *y*-*z* planes of element
x, y, z	: element local axis
X, Y, Z	: system global axis
ν_{12}, ν_{21}	: Poisson ratio
$[D]$	: differential operator matrix
$[E]$	: elasticity matrix
$[G]$	: nodal forces corresponding to assumed stress field
[*N*[	: shape functions
$[P]$	: interpolation matrix for stress
$\{q\},\{\dot{q}\}$	: displacement and velocity components
$\{u\}$	: displacements
$\{\beta\}$	: stress parameters
$\{\sigma\}$	: internal forces
Q_x, Q_y	: internal shear forces per unit length
N_x, N_y, N_{xy}	: membrane forces per unit length
M_x, M_y, M_{xy}	: internal moments per unit length
ρ	: mass per unit volume
ω	: natural circular frequency
ϖ	: non-dimensional frequency
ϕ	: material angle in an element with reference to *x*-axis

Appendix

$$[T]=\begin{bmatrix}
1 & 0 & 0 & 0 & 0 & 0 & 0 & 0 & 0 & 0 & 0 & 0 \\
0 & 1 & 0 & 0 & 0 & 0 & 0 & 0 & 0 & 0 & 0 & 0 \\
0 & 0 & 0 & 1 & 0 & 0 & 0 & 0 & 0 & 0 & 0 & 0 \\
0 & 0 & 0 & 0 & 1 & 0 & 0 & 0 & 0 & 0 & 0 & 0 \\
0 & 0 & 0 & 0 & 0 & 0 & 1 & 0 & 0 & 0 & 0 & 0 \\
0 & 0 & 0 & 0 & 0 & 0 & 0 & 1 & 0 & 0 & 0 & 0 \\
0 & 0 & 0 & 0 & 0 & 0 & 0 & 0 & 0 & 1 & 0 & 0 \\
0 & 0 & 0 & 0 & 0 & 0 & 0 & 0 & 0 & 0 & 1 & 0 \\
\frac{1}{2} & 0 & \frac{(y_1-y_2)}{8} & \frac{1}{2} & 0 & \frac{(y_2-y_1)}{8} & 0 & 0 & 0 & 0 & 0 & 0 \\
0 & \frac{1}{2} & \frac{(x_2-x_1)}{8} & 0 & \frac{1}{2} & \frac{(x_1-x_2)}{8} & 0 & 0 & 0 & 0 & 0 & 0 \\
0 & 0 & 0 & \frac{1}{2} & 0 & \frac{(y_2-y_3)}{8} & \frac{1}{2} & 0 & \frac{(y_3-y_2)}{8} & 0 & 0 & 0 \\
0 & 0 & 0 & 0 & \frac{1}{2} & \frac{(x_3-x_2)}{8} & 0 & \frac{1}{2} & \frac{(x_2-x_3)}{8} & 0 & 0 & 0 \\
0 & 0 & 0 & 0 & 0 & 0 & \frac{1}{2} & 0 & \frac{(y_3-y_4)}{8} & \frac{1}{2} & 0 & \frac{(y_4-y_3)}{8} \\
0 & 0 & 0 & 0 & 0 & 0 & 0 & \frac{1}{2} & \frac{(x_4-x_3)}{8} & 0 & \frac{1}{2} & \frac{(x_3-x_4)}{8} \\
\frac{1}{2} & 0 & \frac{(y_1-y_4)}{8} & 0 & 0 & 0 & 0 & 0 & 0 & \frac{1}{2} & 0 & \frac{(y_4-y_1)}{8} \\
0 & \frac{1}{2} & \frac{(x_4-x_1)}{8} & 0 & 0 & 0 & 0 & 0 & 0 & 0 & \frac{1}{2} & \frac{(x_1-x_4)}{8}
\end{bmatrix}$$